Compact spectrometer system based on a gradient grating period guided-mode resonance filter

Hsin-An Lin, Hsin-Yun Hsu, Chih-Wei Chang, and Cheng-Sheng Huang*

Department of Mechanical Engineering, National Chiao Tung University, 1001 Ta Hsueh Rd., Hsinchu 30010, Taiwan

csh@nctu.edu.tw

Abstract: We demonstrate a compact spectrometer system by using a gradient grating period guided-mode resonance filter—mounted on a linear photodetector array—that exhibits spatially dependent resonance characteristics; a specific incident wavelength is reflected such that the underlying array pixels measure minimum intensity. A precalibrated transmission efficiency matrix is used to determine each pixel's transmission efficiency for specific wavelengths. Unknown spectral information can be calculated from the measured intensity. Grating periods of 250–388 nm in 2-nm increments are used in each 100-cycle period. Device length is 2.23 mm. Spectral range of 506–700 nm is measurable with 1-nm resolution.

OCIS codes: (050.2770) Gratings; (050.6624) Subwavelength structures; (120.6200) Spectrometers and spectroscopic instrumentation; (230.7408) Wavelength filtering devices; (300.6190) Spectrometers.

References and links

1. Z. Xia, A. A. Eftekhar, M. Soltani, B. Momeni, Q. Li, M. Chamanzar, S. Yegnanarayanan, and A. Adibi, "High resolution on-chip spectroscopy based on miniaturized microdonut resonators," Opt. Express **19**(13), 12356–12364 (2011).
2. D. Sander, M. O. Duecker, O. Blume, and J. Mueller, "Optical microspectrometer in SiON slab waveguides," Proc. SPIE **2686**, 100–107 (1996).
3. B. Momeni, E. S. Hosseini, and A. Adibi, "Planar photonic crystal microspectrometers in silicon-nitride for the visible range," Opt. Express **17**(19), 17060–17069 (2009).
4. O. Schmidt, P. Kiesel, S. Mohta, and N. M. Johnson, "Resolving pm wavelength shifts in optical sensing," Appl. Phys. B **86**(4), 593–600 (2007).
5. S. W. Wang, C. Xia, X. Chen, W. Lu, M. Li, H. Wang, W. Zheng, and T. Zhang, "Concept of a high-resolution miniature spectrometer using an integrated filter array," Opt. Lett. **32**(6), 632–634 (2007).
6. N. K. Pervez, W. Cheng, Z. Jia, M. P. Cox, H. M. Edrees, and I. Kymissis, "Photonic crystal spectrometer," Opt. Express **18**(8), 8277–8285 (2010).
7. A. Emadi, H. Wu, G. de Graaf, and R. Wolffenbuttel, "Design and implementation of a sub-nm resolution microspectrometer based on a Linear-Variable Optical Filter," Opt. Express **20**(1), 489–507 (2012).
8. F. Meng, R.-J. Shiue, N. Wan, L. Li, J. Nie, N. C. Harris, E. H. Chen, T. Schröder, N. Pervez, I. Kymissis, and D. Englund, "Waveguide-integrated photonic crystal spectrometer with camera readout," Appl. Phys. Lett. **105**(5), 051103 (2014).
9. J. Bao and M. G. Bawendi, "A colloidal quantum dot spectrometer," Nature **523**(7558), 67–70 (2015).
10. S. W. Wang, X. Chen, W. Lu, L. Wang, Y. Wu, and Z. Wang, "Integrated optical filter arrays fabricated by using the combinatorial etching technique," Opt. Lett. **31**(3), 332–334 (2006).
11. S. S. Wang and R. Magnusson, "Theory and applications of guided-mode resonance filters," Appl. Opt. **32**(14), 2606–2613 (1993).
12. R. Magnusson and S. S. Wang, "New principle for optical filters," Appl. Phys. Lett. **61**(9), 1022–1024 (1992).
13. H.-A. Lin and C.-S. Huang, "Linear variable filter based on a gradient grating period guided-mode resonance filter," IEEE Photonics Technol. Lett. **28**(4), 1042-1045 (2016).
14. R. Magnusson, Y. Ding, K. J. Lee, D. Shin, P. S. Priambodo, P. P. Young, and T. A. Maldonado, "Photonic devices enabled by waveguide-mode resonance effects in periodically modulated films," Proc. SPIE **5255**, 20–34 (2003).
15. H. A. Lin, H. Y. Hsu, and C. S. Huang, "Compact wavelength detection system based on a gradient grating period guided-mode resonance filter," submitted for publication (2016).

#261297 Received 16 Mar 2016; revised 5 May 2016; accepted 9 May 2016; published 11 May 2016

1. Introduction

Conventional spectrometers based on diffraction gratings or prisms can achieve high spectral resolutions by increasing the distance to the detection element for wavelength discrimination. However, they are bulky and must be operated off-chip. Owing to the increasing demand for lab-on-a-chip (LOC), point-of-care, handheld devices and their integration with smartphones, we believe that a strong demand for developing integrated on-chip compact spectrometers is existed. The main challenge in realizing an integrated spectrometer that relies on dispersive components is the trade-off between resolution and structural size [1]. Several compact spectrometers have been proposed to overcome this problem and can be broadly classified into two depending on the direction of the dispersed light: the in-plane type, in which incoming light is diffracted into different in-plane directions [2, 3], and the out-of-plane type, in which the scattered light is coupled out of the chip [1, 4–9]. Different dispersive elements have been demonstrated in these compact spectrometer systems, including grating structures, photonic crystals (PCs), microdonut resonators, and Fabry–Perot (FP) interferometer. 1.2 nm wavelength resolution has been demonstrated when combining superprism and negative refraction effects in the design of the PC compact spectrometer [3]. In other studies, PCs with different lattice constants and designs have been displayed to selectively couple different wavelengths out of substrates [6, 8]. A spectrometer of 60 μm by 8 μm consisting of 24 nanocavities has been showed to achieve 1 nm resolution in the bandwidth of 1522–1545 nm. A linear filter based on FP interferometer as a dispersive element has been attractive and demonstrated by several groups [4, 5, 7]. Multilayered dielectric mirrors on top and bottom of the cavity are often required to have high finesse to achieve high spectral resolutions. By combining photoresist reflowing and etching, Emadi et al. [7] is able to fabricate a tapered cavity thickness that allowed spatially dependent wavelength to be transmitted. By contrast, Wang et al. has developed combinatorial etching technique to fabricate various cavity thicknesses [10]. Xia et al. [1] has developed high Q microdonut resonantors to couple out a specific wavelength from an input waveguide bus. An operating bandwidth of ~50 nm, with ~0.6 nm resolution has been demonstrated. Most aforementioned techniques have been focused on the peak wavelegnth detection, and only a few incorporated algorithms to calculate or reconstruct a spectrum of an input light [5–7]. Recently, Bao and Gawendi [9] demonstrate a spectrometer based on broadband filters, which are realized by colloidal quantum dot (CQD) with various sizes and compositions. With the monochromatic light demonstration, the spectra resolution of 1 nm can be achieved. Thruogh a sophisticated algorithm, they are able to reconstruct an incident spectrum [9]. Various compact spectrometers with their detection range, spectral resolution, and size are summarized in Table 1.

Table 1. Detection range, resolution and size of various compact spectrometers.

Dispersive Element	Detection Range (nm)	Resolution[a] (nm)	Size	Spectrum Reconstruction
Microdonut [1]	1550–1610 (60)	0.6	1 mm ‰ 1 mm	No
FP [4]	700–1000 (300)	<0.001	~9.4 mm	No
FP [5]	722–880 (158)	1.7–3.8	12 mm ‰ 12 mm	Yes
FP [7]	615–680 (65)	0.7	NA	No
FP [7]	580–720 (140)	2.2	NA	Yes
PC [8]	1522–1545 (23)	1	60 μm ‰ 80 μm	No
CQD [9]	360–690 (300)	1	8.5 mm ‰ 6.8 mm	Yes

[a]The resolution is the minimum wavelegnth difference between two monochromatic light that can be distinguished.

For potential applications to integrate with LOC or other sensor chips, we demonstrate an out-of-plane type compact spectromter using a gradient grating period guided-mode resonance filter (GGP-GMRF) as a dispersive element. By combining with a photodetector array in conjunction with a precalibrated transmission efficiency matrix, such compact spectrometer can be realized.

Wang and Magnusson et al. [11, 12] demonstrated the guided-mode resonance (GMR) phenomenon in a planar dielectric waveguide incorporated with a subwavelength grating

#261297 Received 16 Mar 2016; revised 5 May 2016; accepted 9 May 2016; published 11 May 2016

structure. GMR allows external illumination to be coupled into waveguide modes through the phase-matching provided by the grating structure, where the waveguide modes reradiate out of the waveguide in a specular reflection direction and interfere constructively with the directly reflected wave. By contrast, the waveguide mode reradiating in the substrate direction interferes destructively with the directly transmitted wave. The grating can be fabricated atop the waveguide, be embedded in the waveguide, or be placed in other configurations. As long as the guided mode overlaps the grating structure, the mode can be excited and leaked from the waveguide.

By gradually varying the grating period [13], GMR has been demonstrated to function as a linear variable filter and is termed GGP-GMRF. In this study, we apply a GGP-GMRF as a dispersive element and extend its application to spectrometry.

2. Design, fabrication and characterization

A regular GMR functions as a bandstop filter. For normal incidence illumination with a broadband light source, a particular wavelength (resonant wavelength) of light is coupled to waveguide modes and reflected back, whereas the rest of the light is transmitted through. This can be observed experimentally as a narrow band of reflection peak or transmission dip. Based on the second-order Bragg condition [14], the spectral location of the peak or dip corresponding to the resonant wavelength can be calculated by

$$\lambda = n_{eff}\Lambda \tag{1}$$

where λ is the resonant wavelegnth, n_{eff} is the effective index, and Λ is the grating period. The resonant wavelegnth is proportional to the grating period. By varying the grating period laterally [Fig. 1(a)], the GGP-GMRF provides spatially resolved resonance; hence, to function as a dispersive element.

The GGP-GMRF was fabricated using replica molding and film deposition. In brief, a silicon master with gradient grating periods was fabricated through electron-beam lithography and reactive ion etching. The grating period was varied from 250 to 388 nm in increments of 2 nm, and the grating depth was 45 nm. A UV-curable polymer (NOA68, n = 1.556) was sandwiched between the master and a flexible sheet of polyethylene terephthalate (PET) substrate. When NOA68 was cured by exposure to UV light, the NOA68/PET was separated from the master. Lastly, a TiO_2 layer (thickness: 134 nm) was sputter-deposited to complete the plastic GGP-GMRF [Fig. 1(b)]. Figure 1(c) and 1(d) respectively show top and cross-sectional scanning electron microscopy (SEM) views of the finished GGP-GMRF with a grating period of approximately 250 nm and resulting duty cycle of nearly 0.8. Figure 1(e) shows the transmission spectra of TE-polarized light at different locations (or periods); this figure indicates that a linear variable bandstop filter is successfully realized using the fabricated GGP-GMRF. The fabrication and characterization of GGP-GMRF have been detailed in a previous study [13].

#261297 Received 16 Mar 2016; revised 5 May 2016; accepted 9 May 2016; published 11 May 2016

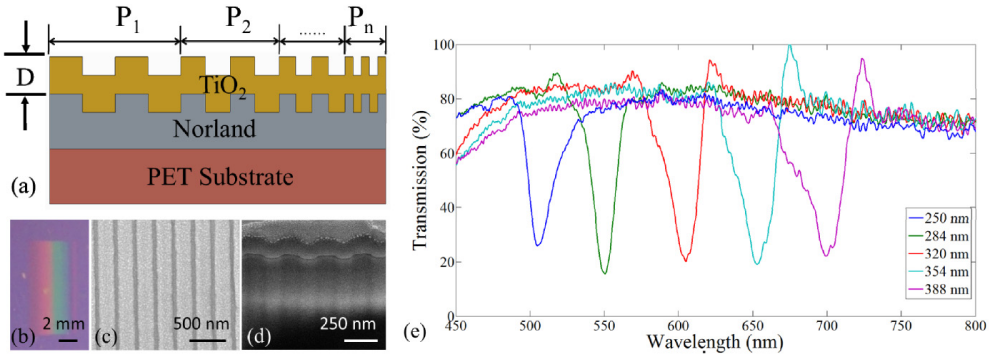

Fig. 1. (a) Schema of GGP-GMRF. (b) Optical image of a completed plastic GGP-GMRF. (c) and (d) SEM images of top and cross-sectional views, respectively. (e) Transmission spectra for different grating periods.

Figure 2 shows the working principle of the proposed spectrometer system. The GGP-GMRF exhibits spatially dependent resonance [Fig. 2(a)]. For single-wavelength illumination [Fig. 2(b)], the incident light excites resonance at a specific location of the GGP-GMRF. Therefore, it will be reflected back at this location and will be transmitted through the remaining regions of the GGP-GMRF. The photodetector beneath the GGP-GMRF measures the intensity profile as a function of pixel locations, as shown in Fig. 2(c). With careful precalibration, the minimum intensity pixel number can be correlated with the incident wavelength [15].

For illumination with a broadband light source, the total intensity measured from each pixel consists of the transmission of its corresponding resonance wavelength in addition to other wavelengths. Owing to the finite full-width half maximum (FWHM) of the resulting resonance at each period, the resulting intensity profile is broadened [Fig. 2(c)] such that the correct spectra information cannot be obtained simply by reversing the intensity profile of the photodetector.

3. Working principle

During precalibration, a specific wavelength of light from the monochromator is illuminated on the GGP-GMRF. The transmission efficiency for each pixel at each wavelength can be obtained to construct the transmission efficiency matrix, T. In this study, T is a j × j matrix; here, the first subscript indicates the resonance region, which is the corresponding pixel with minimum intensity for each calibrated wavelength, and the second subscript refers to a specific wavelength used for calibration. For example, T_{42} represents the transmission efficiency for the 2nd wavelength at the 4th resonant region.

For a known spectrum, I(l), incident on the GGP-GMRF, the light can be digitized to I_j, where the subscript j corresponds to the j^{th} wavelength used for calibration, and the resulting intensity profile on the linear sensor array can be simply calculated using C = TI, where C represents the discrete intensity at each resonance region in the photodetector. By contrast, to find an unknown incident spectrum, its spectral information/intensity profile, I(l), can be calculated or restored [Fig. 2(b)], on the basis of the measured intensity profile in the photodetector, C [Fig. 2(c)], and the precalibrated transmission efficiency matrix, T. In this study, we used the *fmincon* function from the nonlinear optimization toolbox in Matlab to calculate unknown I(l).

#261297 Received 16 Mar 2016; revised 5 May 2016; accepted 9 May 2016; published 11 May 2016

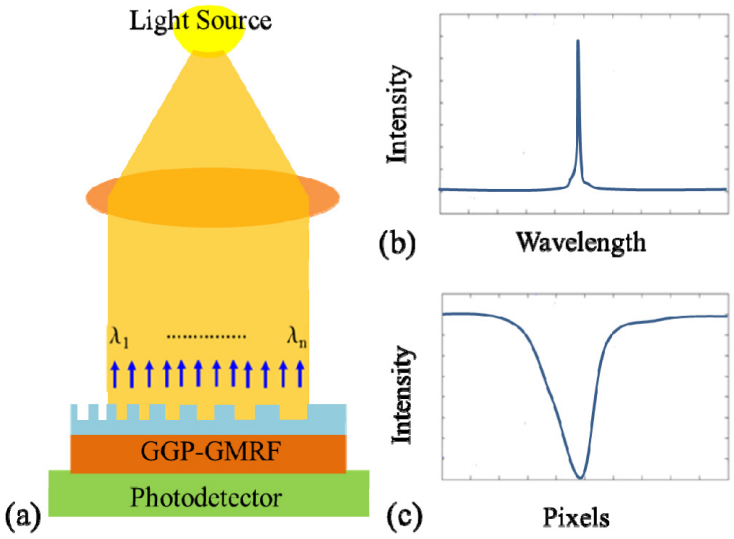

Fig. 2. Fundamental concept of using GGP-GMRF with a photodetector as a spectrometer. (a) Schematic setup of GGP-GMRF spectrometer. (b) Illustration of an incident wave and (c) the corresponding intensity distribution measured in photodetector. Please refer to the text for the detailed description.

4. Calibration

A monochromator (DK242, Spectral Products) incorporated with a broadband light source (LSH-150, Taiwan Fiber Optics, Inc.) was used to generate a specific wavelength of light to characterize the GGP-GMRF and to obtain the transmission efficiency matrix. The monochromator used in this study can generate a wavelength with 2.4-nm FWHM when the slit size is set to 1500 μm.

In this study, the spectral range of 506–700 nm was used to demonstrate the GGP-GMRF spectrometer. The incident light from the monochromator was TE-polarized and expanded to cover the size of the GGP-GMRF. As described earlier, when a specific wavelength of light is incident on the GGP-GMRF, it excites resonance at a specific location. Therefore, the light is reflected back at such locations and transmitted through other locations, resulting in a minimum intensity underneath this location, as shown in Fig. 2(c). Owing to electronic noise, determining the corresponding pixel with the minimum intensity profile for a specific wavelength on the basis of the raw intensity profile measured in the photodetector can be difficult. To overcome this problem, a Lorentzian function is used to fit the intensity profile, as shown in the inset of Fig. 3, which allows us to more accurately determine the corresponding pixel with minimum intensity. The designed GGP-GMRF spectrometer system can distinguish a 1-nm difference based on the CCD intensity profile [Fig. 3], where the corresponding pixel with minimum intensity for five different incident wavelengths, 600–604 nm, can be clearly identified.

As shown in Fig. 3, for each wavelength, there is a corresponding pixel with minimum intensity. The transmission efficiency at such pixel (resonance region) to this resonant wavelength is calculated as a ratio of the intensity at such pixel to the intensity measured at the photodetector without a GGP-GMRF. The transmission efficiency at such pixels to other nonresonant wavelengths can also be calculated as the ratio of the intensity at the pixel when the light is transmitted through the GGP-GMPF to the intensity when the light directly illuminates the pixel.

For example, at 600 nm, the corresponding pixel with minimum intensity (5078.83) is pixel #1289 [Fig. 3]. The transmission efficiency at pixel #1289 for 600 nm is 0.127, which is

#261297 Received 16 Mar 2016; revised 5 May 2016; accepted 9 May 2016; published 11 May 2016

the ratio of 5078.83 to 39785.47 (intensity at pixel #1289 when 600-nm light is illuminated on the photodetector without GGP-GMRF). The transmission efficiency at pixel #1289 for 604 nm is 0.288, which is the ratio of 12003.72 to 41630.9 (intensity at pixel #1289 when 604-nm light is illuminated on the photodetector without GGP-GMRF). The same procedure was performed for all wavelengths in all resonance regions to generate the transmission efficiency matrix.

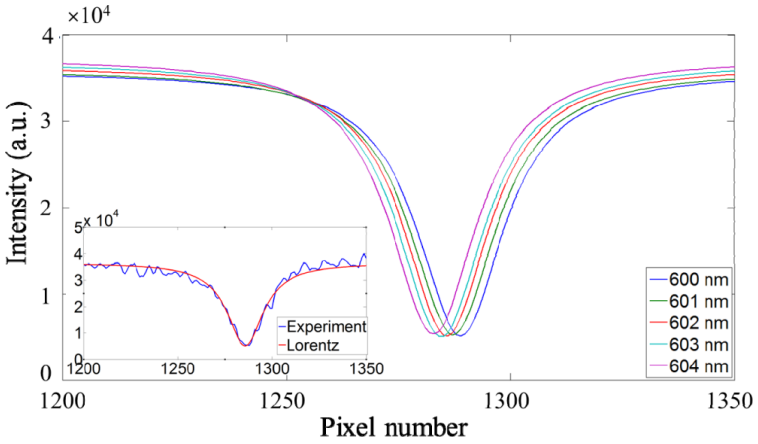

Fig. 3. Lorentzian fitted curves of the intensity distribution measured using the photodetector for different incident wavelengths (600–604 nm). The inset shows the raw intensity distribution and the Lorentzian fitted curve for 600-nm incident light.

5. Experiment verification

Two different types of light sources were used to verify the design and data processing: single-wavelength light from a monochromator and broadband light from a commercial LED. First, three different wavelengths with 2-nm separation from the monochromator were TE-polarized, expanded to cover the entire area of the GGP-GMFR, and illuminated directly onto the GGP-GMRF. Based on the photodetector measurements, as shown in Fig. 3, and the precalibrated transmission efficiency matrix, the calculated spectra based on GGP-GMRF (solid curves) and a commercial spectrometer (USB2000 + VIS-NIR-ES, Ocean Optics) (dotted curves) are presented in Fig. 4. This figure shows that GGP-GMRF can accurately distinguish the peak wavelength with slightly larger line widths, where the FWHMs obtained by the GGP-GMRF are 5–6 nm compared to approximately 2.2 nm in the case of the commercial spectrometer. The absolute intensity is arbitrary between the two systems. The important aspect is the relative intensity between different wavelengths. The Ocean Optics spectrometer indicates that the intensities between different wavelengths have the same magnitude [Fig. 4]. By contrast, the GGP-GMRF spectrometer shows slight variations in the peak wavelength intensity between different wavelengths [Fig. 4].

#261297 Received 16 Mar 2016; revised 5 May 2016; accepted 9 May 2016; published 11 May 2016

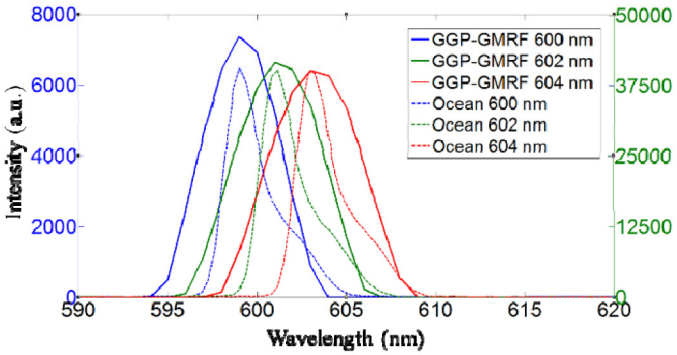

Fig. 4. Three spectra measured using both the GGP-GMRF spectrometer (solid curves) and the Ocean Optics spectrometer (dotted curves). Left and right axes indicate the intensity measured by the GGP-GMRF and Ocean Optics spectrometers, respectively.

In addition to a narrowband light source, we also test a broadband light source from a yellow LED. The setup of the GGP-GMRF for LED testing is shown in Fig. 5(a), where the fiber collimator was used to produce collimated light before its incidence on the GGP-GMFR. Figure 5(b) shows the results obtained from GGP-GMRF (solid curves) and a commercial spectrometer (dotted curves). Again, GGP-GMRF could accurately detect the peak wavelength of 591 nm for the yellow LED with a broader FWHM of 25.50 nm compared with that of 13.80 nm in the case of the Ocean Optics spectrometer.

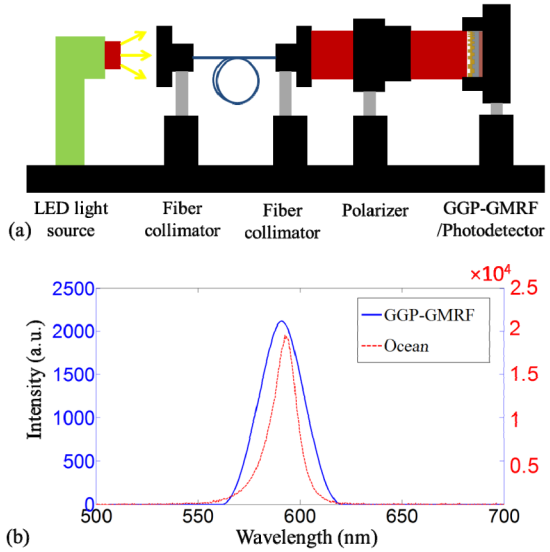

Fig. 5. (a) Experimental setup of GGP-GMRF spectrometer for the LED spectrum measurement. (b) Measured spectra for yellow LED using both GGP-GMRF (solid curves) and Ocean Optics (dotted curves) spectrometers. Left and right axes indicate the intensity measured by the GGP-GMRF and Ocean Optics spectrometers, respectively.

6. Discussion

For both narrow- and broadband light sources, the GGP-GMRF has been demonstrated to successfully detect the peak wavelength. The GGP-GMRF used in this study consists of gradient grating periods with 2-nm increments. Each period consists of 100 cycles, and the GGP-GMRF with the photodetector array used in this work can resolve a 1-nm difference, as shown in Fig. 3. Thus, for a wavelength difference smaller than 1 nm, the minimum intensity

#261297 Received 16 Mar 2016; revised 5 May 2016; accepted 9 May 2016; published 11 May 2016

results in the same pixel. In this case, we can only achieve 1 data point per 1-nm wavelength, which is suspected to be one of the causes for the broader FWHMs obtained by the GGP-GMRF. In addition, this could cause slight variation in the spectral profiles compared with the results obtained from a commercial spectrometer. To achieve better resolution, one could further reduce the increment or increase the number of cycles for each period or use photodetector array with higher resolution.

In addition, the environmental lighting condition during spectrum measurement can be slightly different from that during precalibration, which results in the actual transmission efficiency being slightly different from that in the transmission efficiency matrix obtained during precalibration. Currently, during precalibration, light exiting the monochromator was collimated by a lens before entering the GGP-GMRF/photodetector. By contrast, during measurement, light was collimated using a fiber collimator. Both of these collimation methods show slightly different transmission characteristics; therefore, this results in slightly inaccurate measured spectral information, including both the intensity and the spectral profile, as shown in Fig. 4.

Despite the abovementioned limitation, which can be improved in the near future, the demonstrated device with a footprint of only 2.23-mm long can achieve 1-nm resolution for the detection range of 194 nm, which is very comparable to other spectrometers listed in Table 1. As mentioned previously, for spectrometers based on FP, the fabrication of both multilayered dielectric mirrors and tapered cavity are more complex compared to the demonstrated GGP-GMRF spectrometer. The working principle of the GGP-GMRF and CQD microspectrometer are all based on broadband filters. However, the GGP-GMRF offer couple advatages. The potential batch process can be adapted to scale up the production of the GGP-GMRF with good quality control. The material deterioration and toxicity are not the concern compared to the CQD type.

7. Conclusion

In this work, we demonstrated a GGP-GMRF compact spectromter system, which can measure the peak wavelength with high accuracy and slightly broader FWHMs. A GGP-GMR spectrometer represents a new paradigm that allows high-resolution spectral information to be measured in a compact configuration. The demonstrated device has grating periods of 250–388 nm in 2-nm increments. Each period consists of 100 cycles, and consequently, the total device is only 2.23-mm long. Despite its compact size, the GGP-GMRF can measure wavelengths of 506–700 nm with 1-nm resolution. Such compact spectrometers can be beneficial for handheld measurement system or for LOC or biochip detection.

Acknowledgments

This research was supported by the National Science Council, Taiwan (MOST 103-2221-E-009-075). The authors thank the Nano Facility Center at National Chiao Tung University and National Nano Device Laboratories, Taiwan, for their support in fabricating and characterizing the gradient grating period guided-mode resonance filter.

#261297 Received 16 Mar 2016; revised 5 May 2016; accepted 9 May 2016; published 11 May 2016